5th International Conference on Experimental Fluid Mechanics ICEFM 2018 Munich
Munich, Germany, July 2-4, 2018

Rectilinear surge as a canonical model of reverse flow dynamic stall

Anya Jones[1*], **Phil Kirk**[1]

[1] University of Maryland, Department of Aerospace Engineering, College Park, MD, USA

[*] arjones@umd.edu

Abstract

A two-dimensional representation of reverse flow on a high advance ratio rotor is explored. Experiments were performed on a blade element undergoing sinusoidal oscillations in rectilinear surge. Unsteady surface pressure and flowfield measurements were acquired. The formation and convection of a dynamic stall vortex was observed, specifics of which vary with reduced frequency and advance ratio. The structure of the flow was found to be similar to that in the reverse flow region of a high advance ratio rotor.

1 Introduction

Reversed and separated flow is a common phenomenon in a wide variety of problems. One example of this type of flow occurs on the retreating blade of a high advance ratio rotor where the forward flight speed of the vehicle is greater than the aftward speed of the rotor blade element. Here, the net relative flow is from the geometric trailing edge of the blade to the geometric leading edge of the blade (i.e., reversed).

While the high advance ratio rotor is a well-known example of reverse flow, it is difficult to fully understand the fundamental flow physics of the problem in a case where the blades are subject to many variables simultaneously. In the case of the rotor, for example, the blade element in question also experiences oscillatory changes in angle of attack, yaw angle, and local flow velocity according to changes in the cyclic, inflow, flap angle, and lead/lag Leishman (2006). In order to study the problem of vortex formation and convection more fundamentally, rotor flows may be decomposed into their constitutive components. The vortex that results from a pitching motion, often referred to as a dynamic stall vortex (DSV), has been studied extensively throughout the literature, but most of this work has been conducted in a constant freestream velocity. Because the convection of any vorticity into the wake is greatly dependent on the flow velocity, we would expect the convection of the shed DSV to depend greatly on flow velocity as well. Therefore, while these studies can tell us something about the formation of the DSV, the specifics of its convection in these tests may have limited applicability to real-world kinematics that typically also include a time-varying component of velocity, necessitating investigation of dynamic stall in a time-varying freestream.

Many dynamic stall experiments simplify the complex kinematics present on a rotor to a pure angle of attack oscillation. In a similar way, pure surge experiments can be used to simplify the problem to a velocity oscillation. Like dynamic stall studies, a pure surge experiment represents another way of simplifying flight kinematics while preserving velocity oscillations. For small variations in freestream velocity that allow for attached flow, linear airfoil theory may applied in a quasi-steady manner. In particular, Isaacs (1945) adapted thin airfoil theory to account for these effects in fixed-incidence periodic flows, and Greenberg (1947) simplified and adapted Isaacs' theory by assuming the wake was sinusoidal incorporating the work of Theodorsen (1935). The result of this work was a set of closed form expressions for the lift and moment of an airfoil in attached flow undergoing sinusoidal pitch, surge, and heave.

Experimental work in surge is far less common than that in pitch. In some early work, the time-varying components of velocity were superimposed with pitch oscillations to determine the effect of freestream variability on dynamic stall (Pierce et al., 1978; Favier et al., 1988). Maresca et al. (1979) then conducted an extensive study of pure sinusoidal surge (without pitching) at low and high incidence with variable frequency and amplitude. At high incidence, Maresca observed vortex formation and lift characteristics similar to that traditionally expected from pitch-induced dynamic stall. Recently, Granlund et al. (2016) explored the accuracy of Isaacs' and Greenberg's potential flow models to wings at high and low incidence sinusoidally

surging into and out of reverse flow. Granlund found excellent agreement throughout the velocity cycle at low incidence (even in reverse flow), and surprisingly good agreement at high incidence in the reverse flow region. During high incidence acceleration, however, Granlund found large discrepancies between lift measurements and the model's predictions due to the formation of a vortex similar to that found in dynamic stall.

The present work is a further exploration of surging wing aerodynamics, with a particular focus on the DSV and the forces and pressure distributions that arise due to its formation and convection. Expanding on the work of Maresca et al. (1979), sinusoidal velocity profiles with a wider range of frequencies and amplitudes are explored using particle image velocimetry (PIV), force, and surface pressure measurements, a subset of which are presented here. These results are qualitatively compared to the high-advance-ratio rotor tests of Lind et al. (2017).

2 Methods

Experiments were performed in a $7 \times 1.5 \times 1$ m water-filled tow tank at the University of Maryland, College Park. A towing carriage moved over the length of the tank according to prescribed tow velocity kinematics. The carriage held two linear motors that move along the vertical axis. These vertically moving linear motors were attached to control rods that reached below the surface of the water, where the test model was mounted. The models' speed, pitch, elevation, and rotation were all prescribed through pre-defined functions.

In the current experiments, the model was prescribed velocity kinematics in surge at constant pitch and elevation. The kinematics were similar to the tangential velocity seen by the blade element of a rotor in forward flight

$$v(\phi) = v_0 \left(1 + \lambda \sin(\phi)\right), \tag{1}$$

where v_0 is the average velocity of the sinusoid (i.e. its DC offset), λ is the amplitude of the sinusoid expressed as a ratio to the average velocity, and the variable ϕ gives the position within the sinusoid. In the helicopter analogy, v_0 corresponds to the tangential velocity directly induced by the blade's rotation, λ corresponds to the amplitude of oscillations that arise from forward flight, and ϕ corresponds to the blade azimuth.

Blade oscillation frequency was one variable explored in this experiment. The definition of reduced frequency k for surging wings is given by Greenberg (1947) as

$$k = \frac{\omega_v b}{v_0} \tag{2}$$

where ω_v is the circular frequency of velocity oscillation in rad/s and b is the semi-chord. Recognizing that $\phi = \omega_v t$, the definition of the kinematics could thus also be written as

$$v(t) = v_0 \left[1 + \lambda \sin\left(\frac{k v_0}{b} t\right)\right]. \tag{3}$$

The convective time is also introduced, $t^* = v_0 t/(2b)$, so the blade kinematics can be written most neatly as

$$v(t^*) = v_0 \left[1 + \lambda \sin(2kt^*)\right]. \tag{4}$$

In the current experiments, the average velocity v_0 of the towed wing was fixed and corresponded to an average Reynolds number Re_0 of 40,000. A single wing model was used with a chord of 4.125 in. The velocity sinusoids had amplitude ratios of $\lambda = \{0.25, 0.5, 0.75, 1.0\}$, in combination with reduced frequencies, $k = \{0.16, 0.217, 0.309, 0.511\}$, for a total of sixteen unique kinematic cases, though due to space constraints only a limited subset are presented here. These kinematics were performed for a low incidence at $\alpha = 5^\circ$ and at high incidence with $\alpha = 25^\circ$.

The model towed by these kinematics, shown in Figure 1(a), was a NACA 0012-64 wing with 24 in span and a 4.125 in chord, resulting in an aspect ratio of 5.8. The model was constructed from 15 separate segments, aligned along two stainless steel spars to provide rigidity. One segment, which was 3D printed, housed eight pressure sensors aligned along the chord. Silicon sealant was injected below the sensors and around the sensor ring to prevent leakage. A cap was then placed over the sensor to create a smooth surface. This chordwise row of sensors was 6.75 in (1.6 chord lengths) from the left tip of the wing. The chordwise locations of the sensors are given in Figure 1(b).

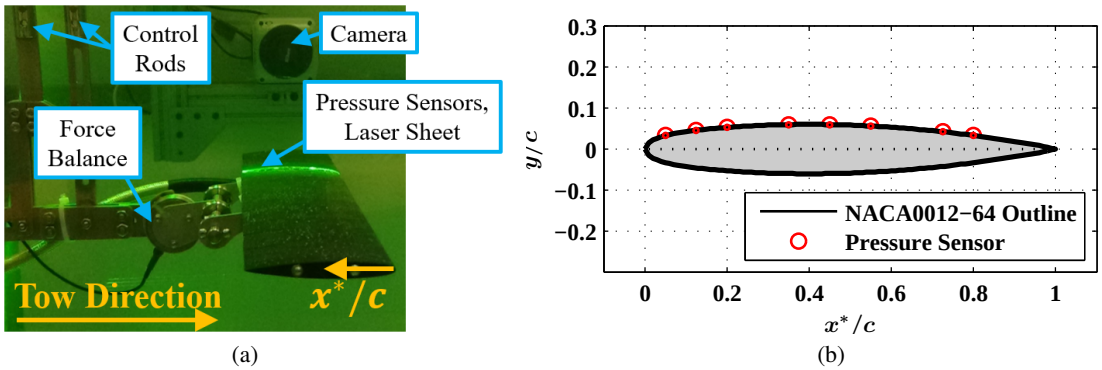

(a) (b)

Figure 1: (a) The model used in these experiments, shown at $\alpha = 0°$. (b) Location of pressure sensors on the wing: $x^*/c = \{0.05, 0.125, 0.2, 0.35, 0.45, 0.55, 0.725, 0.80\}$.

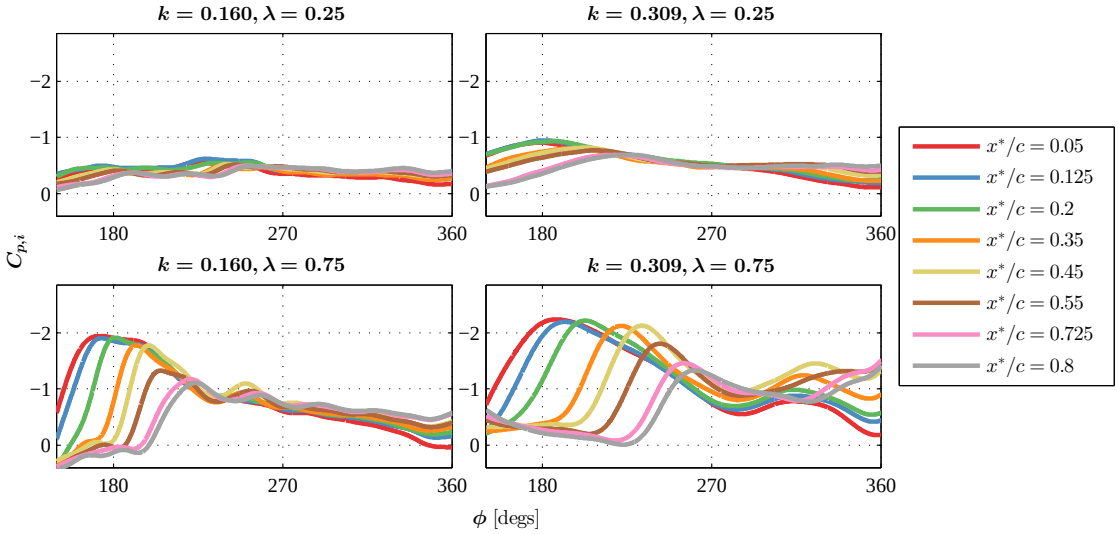

Figure 2: Instantaneous pressure coefficient for a sinusoidally surging wing at $\alpha = 25°$. Note the clear low pressure wave for the $\lambda = 0.75$ cases.

3 Results and Discussion

Experiments on a wing surging with a sinusoidal velocity profile in a water-filled towing tank were performed at two incidence angles ($\alpha = 5, 25°$) and a wide variety of reduced frequencies $k = \omega c/2U_\infty$, and advance ratios $\lambda = 2Ac/k = \mu/(r/R)$. The test model was equipped with a 6-DOF force/torque sensor and unsteady pressure sensors were installed along the wing chord, giving rise to the pressure coefficient measurements shown in Figures 2 and 3. Note that in Figure 2, the measured pressures are reported as instantaneous pressure coefficients, i.e., normalized by the instantaneous dynamic pressure, whereas in Figure 3, the measured pressures are reported as the more conventional pressure coefficient, i.e., normalized by the average dynamic pressure.

At low incidence, low reduced frequency, and/or low advance ratio, Greenberg's linear theory for a sinusoidally surging wing was found to be a good approximation of the unsteady loading on the wing. However, at high incidence and/or for more aggressive wing motions, flow separation resulted in significant departure from linear theory. Figure 2 provides evidence of this phenomenon in the form of instantaneous pressure coefficients, i.e., dimensional pressure normalized by the dynamic pressure at the time of the measurement. In the less aggressive cases ($\lambda = 0.25$), the pressure coefficient varies roughly simultaneously across the

wing chord. However, in the more aggressive cases ($\lambda = 0.75$), unsteady pressure waves become evident after $\phi = 150°$. A large wave of low pressure can be seen to convect along the wing, hitting the sensor closest to the leading edge earliest in the cycle (near $\phi = 150°$) and passing downstream over successive sensors as the cycle progresses.

The convection of this pressure wave can also be visualized by plotting pressure contours as in Figure 3. Here, the *y*-axis shows the chordwise position, the *x*-axis shows the phase angle, and the color scale shows the pressure coefficient (interpolated from sensor measurements at the given locations). In the example shown here, the maximum suction pressure occurs near the midchord of the wing, implying that the pressure wave is not fully developed before it passes the front portion of the wing, and the strength of the pressure wave decreases after it passes the midchord. The suction pressure wave also convects downstream over the wing nearly linearly with phase/time. Convection speed of the pressure wave thus can be easily computed. Similar flow features are observed for a range of k and λ, though with varying intensity, timing, and duration. Some cases result in multiple pressure waves, corresponding to the formation of multiple vortices in a manner similar to that reported by Lind and Jones (2016).

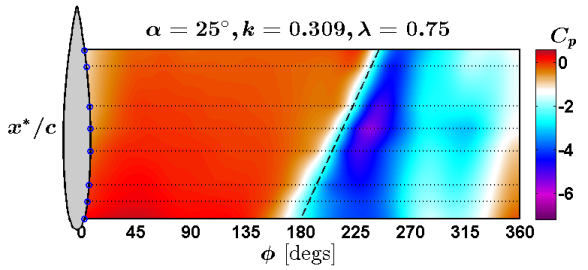

Figure 3: Pressure coefficient for a surging wing. Note the low pressure wave marked with the dashed line.

More information about the pressure wave can be obtained by relating the pressure signals to flow field measurements obtained via PIV. For the case where $\lambda = 0.75$ and $k = 0.309$, the velocity field, vorticity field, and pressure measurements are plotted for multiple phase angles in Figure 4. At $\phi = 180°$, (when the wing is accelerating and at its average velocity), the vorticity field reveals a shear layer separating from near the leading edge and reattaching to the airfoil before the midchord. By $\phi = 210°$, the shear layer has rolled up into a leading edge vortex (LEV) and expanded the region of suction on the airfoil. At $\phi = 240°$, the LEV has convected significantly downstream, almost off the airfoil, and the suction wave has continued with it. At $\phi = 270°$, (the maximum velocity portion of the cycle), the LEV has mostly dissipated and the suction wave has passed, leaving behind a weaker suction pressure that is relatively constant over the wing chord. The flow field remains in this fully stalled state for the remainder of the cycle. In Figure 3, the pressure contours for this case, we saw a linear convection of the suction wave beginning at $\phi = 180°$ and reaching the final sensor at about $\phi = 240°$, which corresponds to the passage of the LEV in the flow field images. The region of large suction caused by the LEV (in dark blue), fades to weaker suction as the LEV dissipates and the wing enters full stall, indicated by a lack of pressure change over both chord and cycle time (a large region of solid light blue).

Results from this canonical surging wing experiment can be compared to flowfield measurements on a high advance ratio Mach-scaled rotor obtained in the Glenn L. Martin Wind Tunnel (GLMWT). Particle image velocimetry (PIV) was used to obtain time-resolved flowfield measurements centered at $\psi = 270°$ for advance ratios $0.6 \leq \mu \leq 0.9$ and a variety of collectives (here, $\theta_0 = 10°$) (Lind et al., 2017). In this work, a strong reverse flow dynamic stall vortex (RFDSV) was observed. The strength and trajectory of this vortex was computed and is shown in Figure 5 for $\mu = \{0.6, 0.7, 0.8, 0.9\}$. The size, strength, and position of the RFDSV vortex bears many similarities to the pressure signature observed in the much simpler surging wing experiments. Compare Figures 4 and 5 (right). Despite the differing wing orientation (i.e., forward flow on the surging wing and reverse flow on the rotor), the overall flow structure remains similar—a strong vortex forms at the leading edge of the wing, followed by eventual separation.

4 Conclusion

Experiments on a two-dimensional blade-element mode of a rotor were performed. The formation and convection of a strong dynamic stall vortex was observed on a wing undergoing sinusoidal surging oscillations representative of a rotor blade element. Similar flow evolution has been observed in rotor experiments, suggesting that ongoing efforts to develop low order models for load prediction in highly separated flows based on canonical two-dimensional experiments might be leveraged for application to more complex and

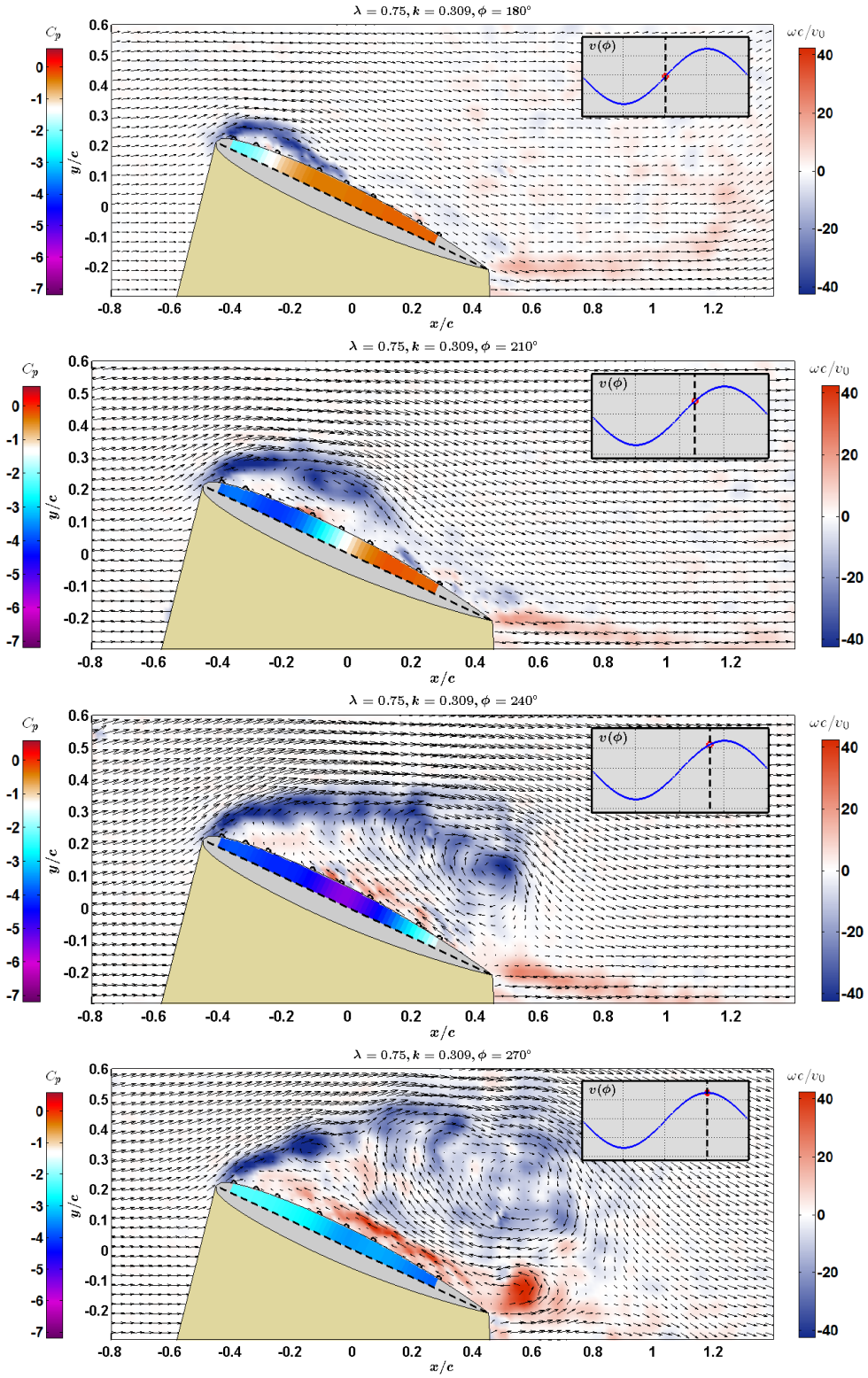

Figure 4: Evolution of LEV and suction wave with $k = 0.309$ and $\lambda = 0.75$, viewed with the vorticity field, velocity field, and surface pressure measurements

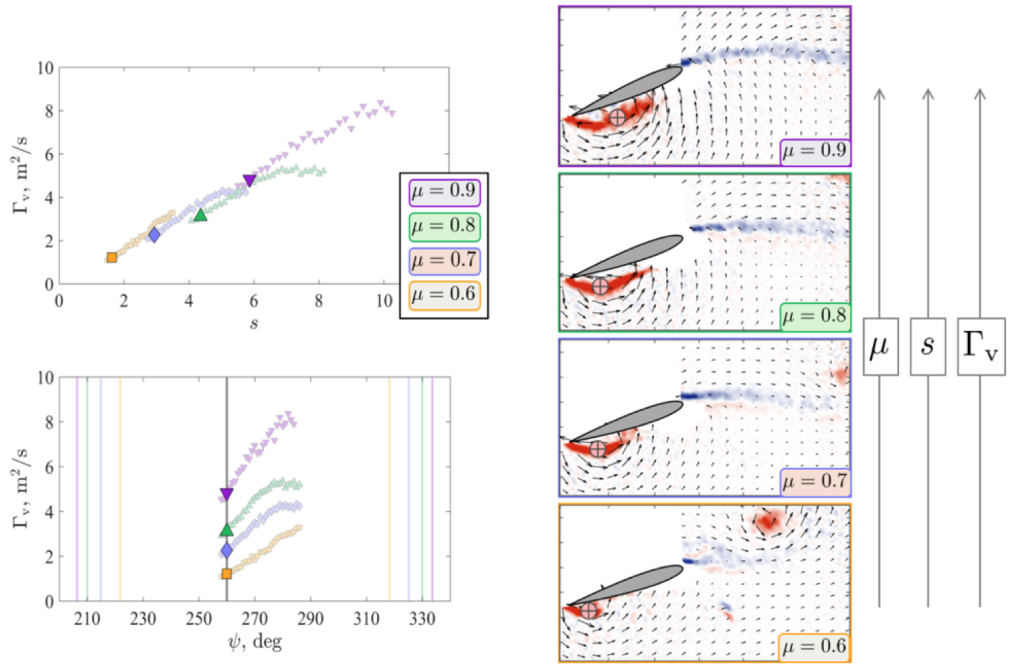

Figure 5: Flowfield measurements on a Mach-scaled high advance ratio rotor. Variation of vortex strength with reduced time (Top left), variation of vortex strength with azimuthal position (Bottom left), and vorticity fields at 260 deg azimuth (Right). Note that for a fixed azimuthal position, as advance ratio increases, the reduced time over which the blade has experienced reverse flow also increases, as does the instantaneous vortex strength. Adapted from Lind et al. (2017).

three-dimensional scenarios, including high advance ratio rotors. Future rotor experiments will provide a more quantitative comparison of the two flows.

Acknowledgements

This work was supported in part by the National Science Foundation under grant 1553970 and the U.S. Army/Navy/NASA Vertical Lift Research Center of Excellence Cooperative Agreement with Mahendra Bhagwatserving as Program Manager and Technical Agent, grant number W911W6-17-2-0004.

References

Favier D, Agnes A, Barbi C, and Maresca C (1988) Combined Translation/Pitch Motion—A New Airfoil Dynamic Stall Simulation. *Journal of Aircraft* 25:805–814

Granlund KO, Ol MV, and Jones AR (2016) Streamwise Oscillation of Airfoils into Reverse Flow. *AIAA Journal* 54:1–9

Greenberg JM (1947) Airfoil in Sinusoidal Motion in a Pulsating Stream. Technical report. NACA

Isaacs R (1945) Airfoil Theory for Flows of Variable Velocity. *Journal of the Aeronautical Sciences,* 54

Leishman JG (2006) *Principles of Helicopter Aerodynamics, 2nd ed.*. Cambridge Univ. Press, New York

Lind AH and Jones AR (2016) Unsteady Aerodynamics of Reverse Flow Dynamic Stall on an Oscillating Blade Section. *Physics of Fluids* 28

Lind AH, Trollinger LN, Manar FH, Chopra I, and Jones AR (2017) Flowfield Measurements of Reverse Flow on a High Advance Ratio Rotor. in *43rd European Rotorcraft Forum*

Maresca C, Favier D, and Rebont J (1979) Experiments on an Aerofoil at High Angle of Incidence in Longitudinal Oscillations. *Journal of Fluid Mechanics* 92:671–690

Pierce GA, Kunz DL, and Malone JB (1978) The Effect of Varying Freestream Velocity on Airfoil Dynamic Stall Characteristics. *Journal of the American Helicopter Society* 23

Theodorsen T (1935) General Theory of Aerodynamic Instability and the Mechanism of Flutter. Technical report. NACA